# Experimental investigation on the effect off near walls on the eigen frequency of a Low Specific speed Francis Runner

Petter T. K. Østby[a,b,*], Kjell Sivertsen[a], Jan Tore Billdal[a], Bjørn Haugen[b]

[a] *Rainpower Norge AS, 2027 Kjeller, Norway*
[b] *NTNU, Richard Birkelands vei 2B, 7491 Trondheim, Norway*

**Abstract**

The importance to correctly predict the natural frequency of a turbine runner have been demonstrated several times. It is now common practice to include the added mass effect of the surrounding water when calculating the natural frequencies. In this paper the added mass effect of water on a simplified low specific speed francis turbine runner is experimentally investigated. Three cases are investigated. 1: The runner hanging in air. 2: The runner hanging in a tank of water. 3: The runner installed into the turbine housing. The measurements reveal a frequency reduction of about 40% when the runner is hanging in water. Installing the runner into the turbine housing does not significantly change the natural frequency of the main blade modes. Modes which vibrate heavily on the outside of the runner are visible in the water tank but becomes dampened when installed into the turbine housing.

*Keywords:* Modal testing, Francis runner, Added mass, Nearby walls, Fluid-structure interaction

## 1. Introduction

The importance to correctly predict the natural frequency of a turbine runner have been demonstrated by several authors[21, 5, 4]. Some turbines have failed very quickly due to resonances in the runner. The 250 MW Svartisen A1 turbine failed in only hours after being put in operation [11] It is now common practice to include the added mass effect of the surrounding water when calculating the natural frequencies.

Nearby ridgid structures are known to increase a fluids added mass and thereby reducing the eigen frequency of the oscillating structures. Fritz [7] showed that the added mass is inversely proposional to the clearance between

*Tel: +47 484 63 485
Email: petter.oestby@rainpower.no

a cylinder and a rigid outer wall. Rodriguez et. al. [15] showed that for a thin plate submerged in water both the plate thickness and distance from nearby walls affect the added mass effect, while also showing that numerical models can predict this effect on simple structures. Bossio et. al. further expanded on the numerical calulation of a disc submerged in water [3]. This is especially important for hydro turbines where the relative clearance (clearance divided by seal radius) between the runner and the surounding components in the seal areas are in the range of 0.1%. Tanaka [18] showed through experiments that reducing the clearance radially and axially on a high head pump turbine reduce the eigen frequency of the runner. Valentín et. al. [22] showed numerically a clear reduction of the natural frequencies of a low head Francis runner as the gaps around the runner was reduced.

Whether or not the a runner will be affected by the nearby walls is dependant on the shape of its eigen modes. These mode shapes will differ between runners of different designs. Several authors have published mode shapes of actual Francis and pump turbine runners with different spesific speeds. [23, 10, 8] The overall trend seems to be that low head runners have more radial motion on the runner band near the outlet, while high head runners have larger disc like mode shapes. These runners may thus be affected differently by the walls.

In this article, the effects of water and covers are experimentally investigated on a simplified low specific speed runner. The effects are evaluated for the first harmonics of the different nodal diameters of a high head runner. The novelty of this article is the measurement of the runners natural frequency while installed in the turbine housing. This article may provide some insight to the questions asked by Trivedi [21, 20]; how the runner housing influences the natural frequencies and damping of a turbine runner. Further, the excitation method, controlling which nodal diameter to excite, is new. At least for hydro turbine runners. The results are then compared to the numerically calculated values using commercial software.

## 2. Experimental setup

The experiment was conducted in Rainpowers Turbine Laboratory in Trondheim, Norway.

### *2.1. Geometry*

The geometry tested is based on a real low specific speed hydro turbine runner ($N_{QE} = 0.066$) with some simplifications to the blade design. It is scaled to a model size with a outlet diameter ($D_2$) of $300mm$. The runner is made of 6 full blades and 6 splitter blades and is CNC machined out of a single block of stainless steel. Model turbines are often made with bolted connections between the runner vanes and the hub/shroud. Fabricating it from a solid block removes uncertainties due to such bolt connections. See Figure 1 for a cross section of the runner.

$$N_{QE} = \frac{nQ^{0.5}}{(gH)^{0.75}} \tag{1}$$

Each vane is a straight foil placed vertically between hub and band. Each 8.3 mm thick near the inlet and taper down to 4.0 mm at the trailing edge. Both the leading edge and trailing edge is profiled with a smooth hydraulic profile and the blades have a 2 mm fillet towards hub and band. The full and splitter blades have cord length 184.7 mm and 93.9 mm respectively. The geometry resemble the simplified model in which Huang et. al. [9] investigated the added mass effects of water.

To test the effect of water on the resonance frequencies of the runner, three different experimental setups were used. First, the runner was suspended on chains hanging in air. In the second test series, the runner was still hanging on the chains but submerged in a tank full of water, as shown in Figure 2a. Only one runner position in the tank was tested. The last test was performed with the runner installed in the water filled turbine housing. A Francis turbine has regions on the outside of the runner called labyrinth seals, where the clearance towards the stationary covers is small. This is done to limit the flow going around the runner. For this turbine the radial clearances towards the stationary seals were $0.17mm.$ and $5.4mm$ towards the upper and lower cover, as shown in Figure 2b.

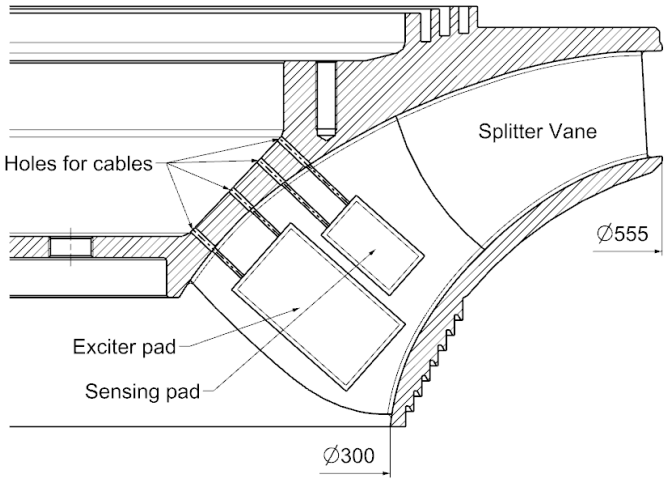


Figure 1: Runner Cross Section

*2.2. Excitation*

Each full vane is equipped with two Piezoelectric pads, one which excites the vane and one which senses the vibrations. Both pads are glued into caveties machined into the runner vane and covered with epoxy. The setup is similar

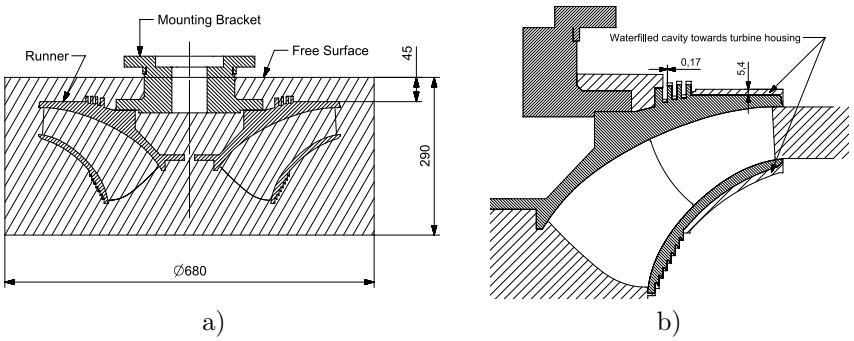


Figure 2: Runner in turbine housing and water tank - Cross Section

to the setup used by other authors investigating added mass and damping of submerged structures [17, 24, 2].

Both the exciter and sensing pads are made of Macro Fiber Composite (MFC) materials which contract and expand when exposed to a changing voltage field. The pads can also be used as high sensitivity strain gauges as they produce voltage differential when expanded. This makes such pads ideal for Multi Input Multi Output (MIMO) modal testing as shown by Ruggiero et. al. [16] and Presas et. al. [12]. Both sets of pads used were made by Smart Materials and are of the type MFC P1 capable of operating between -500 V and 1500 V input voltage. The M5628-P1 was used as exciter pads and M4312-P1 as sensing pads

The exciter pads are controlled by two voltage output modules from National Instruments whose signal is amplified using a high voltage amplifier by Smart Materials. The signal from the sensing pads is logged using two voltage input modules also from National Instruments. All is controlled and logged by Lab View software.

Each nodal diameter (ND) of the runner has a distinct phase angle, $\phi = \frac{2\pi\, ND}{Z_r}$, between each symmetric group [19]. Therefore, by carefully choosing the phase angle between the exciting pads on each vane, every nodal diameter can be excited independently of the others. This method is similar to the traveling wave response method described by Feiner et al. [6]. Possible non-symmetries in the geometry or exciter equipment may excite other nodal diameters as well. Since the runner is excited on the trailing edge of runner vanes, only the modes which oscillate in this region will be excited.

### *2.3. Measurement and processing of data*

The tests are conducted using a stepped sine sweep method. All exciter pads vibrate at the same frequency, each phase shifted $\phi$ from the last. The tests are run from far below ($500Hz$) the resonance frequency to far above ($2000Hz$) the first harmonic in steps of 5 Hz. Each step is held for 1 second before moving to the next. Given that the resonance frequencies are in the range of 1000 Hz this

Figure 3: Left: Pads glued into the vane, Right: Runner ready for geometry measurement

gives enough time for the vibration to settle down to a periodic form. The sine signal is updated at a rate of 40 kHz.

For each frequency step the voltage levels from the sensing pads and a monitor signal from the exciting pads are collected at 10 kHz. Only the second half of each time step is run through an FFT algorithm and the real and imaginary component at the exciting frequency is stored. Using only the second half ensures that transient effects are dampened and only a steady signal is analysed.

*2.4. Calculation of natural frequency and damping*

The measured data is fitted to a transfer function on the form of a rational polynomial function (RPF), defined as Equation (2), using a least squares approach. A method developed by Formenti et. al. [13].

$$H(\omega) = \frac{\sum_k^m b_k s^k}{\sum_k^n a_k s^k}|_{s=j\omega} \tag{2}$$

Using a root finding algorithm on the constants in the denominator $a_k$ the poles $P_k$ of the transfer function can be found. The natural frequencies and damping are then calculated through Equations (3)

$$\begin{aligned} \zeta_k &= -\frac{\Re\{P_k\}}{|P_k|} \\ \omega_k &= |P_k| \end{aligned} \tag{3}$$

Before the RPF estimation,the FFT data from the measurement is rotated back according to the phase angle $\phi$ of the excited nodal diameter. This makes the response from all sensor pads move in phase with each other for the excited nodal diameter. Any other response from nodal diameters not directly excited will thus be cancelled out due to their sum being zero.

$$\sum_{i=0}^{n} sin(\phi + \omega t) = \begin{cases} 0 & \text{if } \sum \phi = 2\pi i, i = 1, 2, 3.. \\ n \cdot sin(\omega t) & \text{if } \sum \phi = 0 \end{cases} \tag{4}$$

Figure 4 shows an example of the method applied to the runner suspended in air excited at ND2. The two first modes are clearly visible and their frequencies

are calculated to be $1073 \pm 0.2Hz$ and $1755 \pm 0.2Hz$ while the damping are calculated to be $0.06\% \pm 0.09\%$ and $0.2\% \pm 0.023\%$ respectively. The uncertainty is based on the covariance matrix returned from the curve fit and the method propagation of uncertainty.

The admittance spike at $1350Hz$ in Figure 4 is the response of other nodal diameters, in this case ND3, resonating even though they do not match the input phase angle. This is likely due to non-symmetries in both the geometry and the excitation equipment. It does however not affect the RPF due to the rotation of the measurement values and the sum if its contribution from all 6 sensors thus being close to 0.

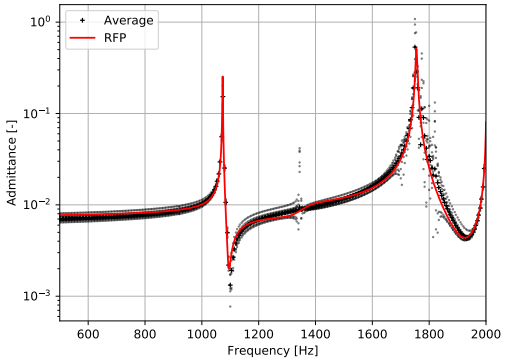


Figure 4: Example of the measured frf data and the RPF function. Nodal Diameter 2 with the runner in air. The spread in data is from the 6 different pads overlaid

## 3. Results

Using the method described above the natural frequencies and damping for the runner was calculated for the tree different setups; hanging in air, lowered into a water tank and placed in the turbine housing. The RPF algorithm captures all major eigen modes with large admittance responses. Small and nearby modes can, through the curve fit process, be joined and the algorithm assumes that they are a single mode. Even smaller modes are not captured at all. This is however not a significant problem as it is the modes with the largest vibrations which are of most importance. The results are shown in Table 1.

As there is only one sense pad on each vane, it is not possible to differentiate between different mode shapes with the same nodal diameter. To be able to calculate the frequency reduction ratio $f_{rr} = 1 - {}^{f_{water}}/_{f_{air}}$ a numerical modal calculation was performed.

Table 1 contains a column of mode types which classifies the mode shapes into categories: "Torsion" is big torsional modes between the runner hub and band. "Blade" are modes mainly in the runner blades. "Disc" are big modes

with clear diameters lines, typically found in circular discs. "Mix" is a combination of "Blade" and "Disc". Examples of the modeshapes are shown in Figure 5

Table 1: Measurement results

| | ND | Frequency [Hz] | ±[Hz] | Damping [%] | ±[%] | Mode Type | Numerical Value [Hz] | Relative Error $f_{num}/f_{meas}-1$ |
|---|---|---|---|---|---|---|---|---|
| Air | 0 | 920.4 | 0.3 | 0.0 % | 0.0 % | Torsion | 921.4 | 0.11 % |
| | 0 | 1778.5 | 0.2 | 0.2 % | 0.0 % | Blade | 1821.3 | 2.41 % |
| | 1 | 1703.9 | 0.7 | 0.5 % | 0.1 % | Disc | 1518.4 | -10.89 % |
| | 1 | 1798.2 | 0.7 | 0.4 % | 0.1 % | Blade | 1820.4 | 1.23 % |
| | 2 | 1073.2 | 0.2 | 0.1 % | 0.0 % | Disc | 1100.0 | 2.50 % |
| | 2 | 1755.1 | 0.2 | 0.2 % | 0.0 % | Blade | 1807.0 | 2.96 % |
| | 2 | 2002.7 | 8.4 | 0.0 % | 0.5 % | Mix | 2066.9 | 3.21 % |
| | 3 | 1346.3 | 0.3 | 0.1 % | 0.0 % | Disc | 1369.5 | 1.72 % |
| | 3 | 1820.2 | 0.1 | 0.1 % | 0.0 % | Blade | 1858.8 | 2.12 % |
| Water | 0 | 890.4 | 1.7 | 0.5 % | 0.0 % | Torsion | 898.7 | 0.93 % |
| | 0 | 1150.8 | 0.1 | 0.1 % | 0.0 % | Blade | 1170.8 | 1.74 % |
| | 1 | 1086.9 | 0.3 | 1.0 % | 0.1 % | Blade | 1085.3 | -0.15 % |
| | 1 | 1472.9 | 9.7 | 2.9 % | 0.7 % | Mix | 1490.0 | 1.16 % |
| | 1 | 1851.9 | 11.1 | 2.3 % | 0.6 % | Blade | 1853.1 | 0.07 % |
| | 2 | 906.5 | 0.7 | 0.6 % | 0.1 % | Mix | 945.9 | 4.35 % |
| | 2 | 1014.2 | 1.0 | 1.7 % | 0.1 % | Blade | 979.1 | -3.46 % |
| | 2 | 1681.3 | 3.3 | 0.4 % | 0.1 % | Mix | 1716.0 | 2.07 % |
| | 2 | 1844.1 | 2.9 | 0.9 % | 0.2 % | Blade | 1865.0 | 1.14 % |
| | 3 | 975.8 | 0.3 | 0.3 % | 0.0 % | Blade | 982.5 | 0.68 % |
| | 3 | 1642.3 | 0.5 | 0.1 % | 0.0 % | Mix | 1645.0 | 0.16 % |
| | 3 | 1802.4 | 1.3 | 0.3 % | 0.1 % | Blade | 1800.2 | -0.12 % |
| Turbine Housing | 0 | 1041.3 | 0.3 | 0.2 % | 0.1 % | Mix | 1108.0 | 6.40 % |
| | 0 | 1151.0 | 0.1 | 0.3 % | 0.0 % | Blade | 1164.6 | 1.18 % |
| | 1 | 1061.7 | 0.5 | 1.6 % | 0.2 % | Blade | 1054.2 | -0.70 % |
| | 1 | 1845.7 | 17.6 | 2.5 % | 1.0 % | Unknown | NA | NA % |
| | 2 | 990.5 | 0.3 | 2.2 % | 0.0 % | Blade | 966.5 | -2.42 % |
| | 2 | 1598.0 | 44.4 | 8.9 % | 2.4 % | Unknown | NA | NA % |
| | 2 | 1816.5 | 120.7 | 15.5 % | 9.3 % | Unknown | NA | NA % |
| | 3 | 973.8 | 0.1 | 1.6 % | 0.0 % | Blade | 957.6 | -1.67 % |
| | 3 | 1646.9 | 9.2 | 5.4 % | 0.7 % | Unknown | NA | NA % |
| | 3 | 1847.5 | 15.8 | 1.2 % | 0.0 % | Unknown | NA | NA % |

### *3.1. Numerical calculation*

A numerical calculation of the modes was performed to identify the different modes found in the experiment.

As the methods to perform numerical eigen frequency analysis with added mass from water are well documented both by several authors [21, 5] and by the user manual of the software (Ansys v18.0) used [1], all details of the simulation will not be given here.

Since the problem is cyclic symmetrical, only 1/6th of the runner is included in the analysis. The water is modelled with acoustic elements and a FSI interface is used on the boundary between the runner and water. All material properties used are shown in Table 2. The numerical model does not include the piezo pads nor the epoxy resin used to mount them. The pads and resin have a density almost matching that of water and the Young modulus of the resin is in the range of 2 MPa. Disregarding these will ignore some stiffness in the model and it may thus underpredict some of the natural modes. A mesh independent study was conducted with the runner in the water tank. Figure 6 shows the effect mesh size has on the numerical results. Mesh independency is reached with cells at 10 mm. All mesh elements are tetraheder elements. With 10mm mesh elements the relative error in frequency is less than 5% for almost all modes.

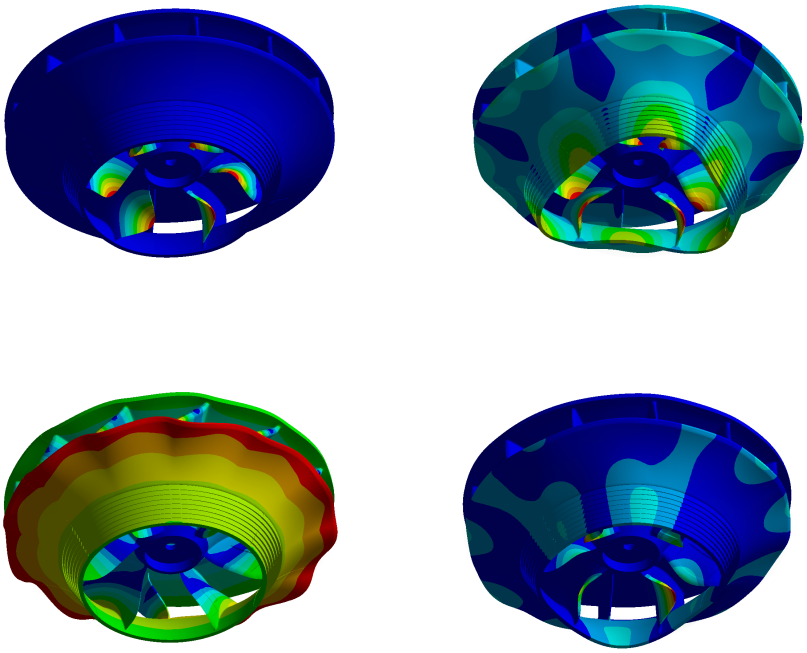

Figure 5: Examples of different modeshapes. From top left going clockwise: Blade, Disc, Mix, Torsion

### *3.2. Discussion*

#### *3.2.1. Frequencies*

Using the mode shapes found by the numerical calculation the frequency reduction ratio of the blade modes was calculated. The results are shown in Table 3. It shows a small but clear reduction in the frequency with increasing nodal diameter. The found frequency reductions are somewhat larger than the findings of Rodriguez [14], although he also found similar reductions with increased nodal diameter.

Inserting the runner into the turbine housing further enhances the frequency reduction for the first blade modes, however not by much. The maximal reduction is found for Nodal Diameter 2 and 3 with 1.4 %. This change is rather small even though the distance from the runner to nearby walls and free surfaces changes significantly from the tank to the housing as can be seen in Figure 2. The frequency reduction ratio is not calculated for the other modes as it is not possible to positively identify the same modes between the tests in the water tank and housing. The FRFs looses their distinct peaks for non-blade modes with the runner inside of the turbine housing as the admittance drops by more

Table 2: Material properties used in calculation

| | | |
|---|---|---|
| Steel | | |
| Young Modulus | 200 | GPa |
| Density | 7650 | $kg/m^3$ |
| Poisson ratio | 0.3 | |
| Water | | |
| Density | 1000 | $kg/m^3$ |
| Speed of sound | 1450 | m/s |

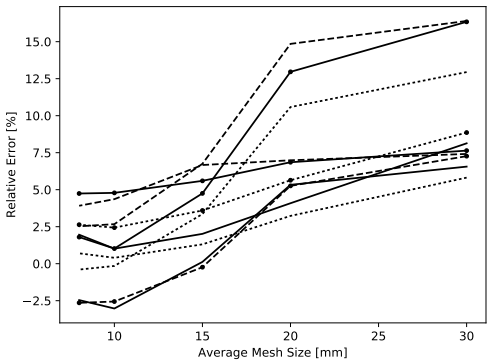


Figure 6: Relative error $f_{calc}/f_{measured} - 1$ for different mesh sizes

than one decade and becomes almost flat. The RFP algorithm is therefore not able do make an estimate for the frequencies or damping with any certainty. Even though the numerics predict mix and disc modes in the frequency range, it is not possible to connect them to the minuscule peaks on the FRFs due to the uncertainty of both the numerics and measurements.

Even though it is not possible to make a quantitative evaluation of the housings effect on the disc and mix modes, it is however worth noticing how the FRFs change with the runner installed in the turbine housing. While the runner is in the air, modes of all types are excited and vibrate heavily. When lowered into the water tank the Blade modes become more predominant while places in the housing only the first blade mode is clearly excited. This seem to apply for all nodal diameters.

The reason for the change in behaviour of the disc and mix modes with the runner in the housing is unclear, but these modes all have large deformations on the hub, band and sealing areas. This means that they will be more affected by the presence of the turbine housing. As these modes vibrate, they move the water in the small spaces outside of the runner which may create both an significant added mass effect and significant viscous damping. Based on

this it is likely that the modes either have shifted their frequency outside of the measurement range due to significant added mass or their damping has increased to a level where the individual peaks cannot be detected. Comparing the results with the numerical calculation it is likely that the latter is the main factor as the numerics does not predict any change in frequency which would shift the modes outside of the measuring range. Had the runner been equipped with sense pads on the hub and band it would probably be easier to quantify the housings effect on the disc and mix modes.

Table 3: Frequency reduction ratios ( $f_{rr}$ [%] ) for the 1st blade mode of different nodal diameters

| Nodal Diameter | In Tank | Housing |
|---|---|---|
| 0 | 35.3 | 35.3 |
| 1 | 39.6 | 41.0 |
| 2 | 42.2 | 43.6 |
| 3 | 46.3 | 46.5 |

*3.2.2. Damping*

The change in measured damping for the first blade mode is shown in Figure 7. It is evident that the damping increases when the runner is lowered into the water for all modes except Nodal Diameter 0. The increase is expected as the viscosity of water in larger than for air. Moving the runner into the turbine housing further increases the damping of all modes. Most likely due to increased water velocities as the space around the runner is reduced. One interesting observation is the low damping observed for Nodal Diameter 0. Even with the runner installed into the turbine housing the damping is 0.3% while it is above 1.5% for all the other modes. The reason for the low damping for ND 0 is unknown, but a hypothesis is that it is due to the blades all moving in phase with each other and thus not creating significant motion of the water relative to the blades.

## 4. Conclusion

Measurements of the eigen frequency and damping of a model size runner was done in three different environments; air, water and inside of the turbine housing. A clear frequency reduction due to the added mass was observed when moving the runner from air to water. The frequency reduction for the main blade modes was in the range of 35.3% to 46.5% increasing with nodal diameter. Moving the runner into the turbine housing had little effect on the measured eigen frequency of the first blade modes of each nodal diameter, only reducing it by a few extra percentages. As for eigen modes with large deformations on the hub and band, moving the runner into the housing had significant effect. In the water tank the modes was clearly visible in the FRF, but when installed into the

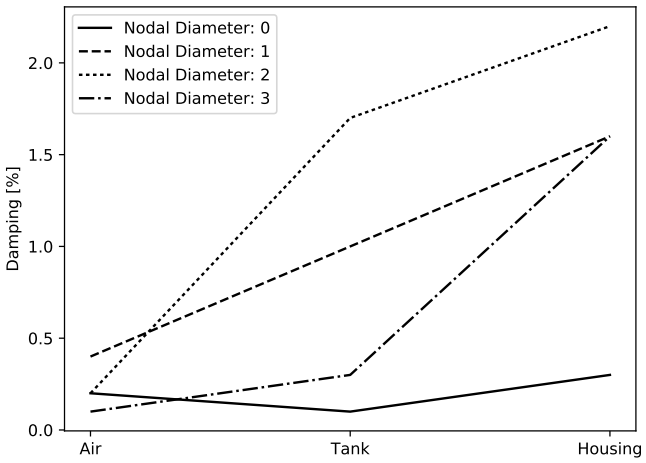


Figure 7: Damping for the first blade mode in the different setups

runner housing the modes could not be detected. Whether this is due to a large shift in frequency or a significantly increased damping is not known. Either way, this experiment shows that it is very important to include the turbine housing when dealing with modes with large deformations on the hub and band. For blade modes the effect of the housing is minimal.

The measured damping increased from almost zero to above 1.5% for all the main blade modes except for Nodal Diameter 0.

Using commercially available software it was possible to calculate the measured eigen frequencies to within ±5% for almost all modes. Some modes had larger deviations, but it is likely due to the boundary conditions where the chain holds the runner.

## 5. Acknowledgements

I would like to thank the Norwegian Research Council for their financial support of this research through their "EnergiX" and "Industrial-Ph.D" grants.

## References

[1] ANSYS Inc. *ANSYS Mechanical, v18.2, Help system,*, 18.2 edition.

[2] Carl W. Bergan, Bjørn W. Solemslie, Petter Østby, and Ole G. Dahlhaug. Hydrodynamic damping of a fluttering hydrofoil in high-speed flows. *International Journal of Fluid Machinery and Systems*, 11(2):146–153, 2018.

[3] Matias Bossio, David Valentin, Alexandre Presas, David Ramos Martin, Eduard Egusquiza, Carme Valero, and Monica Egusquiza. Numerical study on the influence of acoustic natural frequencies on the dynamic behaviour of submerged and confined disk-like structures. *Journal of Fluids and Structures*, 73(Supplement C):53 – 69, 2017.

[4] Andre Coutu, Roy MD, Monette C, and Nennemann B. Experience with rotor-stator interactions in high head francis runner. *Proceedings of the 24th IAHR symposium on hydraulic machinery and systems*, page 10, 2008.

[5] Eduard Egusquiza, Carme Valero, Quanwei Liang, Miguel Coussirat, and Ulrich Seidel. Fluid added mass effect in the modal response of a pump-turbine impeller. (48982):715–724, 2009.

[6] D. M. Feiner, J. H. Griffin, K. W. Jones, J. A. Kenyon, O. Mehmed, and A. P. Kurkov. System identification of mistuned bladed disks from traveling wave response measurements, 2003.

[7] R. J. Fritz. The effect of liquids on the dynamic motions of immersed solids. *Journal of Engineering for Industry*, 94(1):167–173, February 1972.

[8] X Huang, C Oram, and M Sick. Static and dynamic stress analyses of the prototype high head francis runner based on site measurement. *IOP Conference Series: Earth and Environmental Science*, 22(3):032052, 2014.

[9] X X Huang, E Egusquiza, C Valero, and A Presas. Dynamic behaviour of pump-turbine runner: From disk to prototype runner. *IOP Conference Series: Materials Science and Engineering*, 52(2):022036, 2013.

[10] C Müller, T Staubli, R Baumann, and E Casartelli. A case study of the fluid structure interaction of a francis turbine. *IOP Conference Series: Earth and Environmental Science*, 22(3):032053, 2014.

[11] Grunde Olimstad. Løpehjulssprekker på svartisen - beskrivelse av hendelsen og årsak (runner cracks at svartisen -description of event and causes). In *Produksjonsteknisk konferanse*, 2013.

[12] Alexandre Presas, David Valentin, Eduard Egusquiza, Carme Valero, Mònica Egusquiza, and Matias Bossio. On the use of pzt-patches as exciters in modal analysis: Application to submerged structures. In *Proceedings of the 3rd International Electronic Conference on Sensors and Applications*, volume 1, 2016.

[13] David Formenti & M.H. Richardson. Parameter estimation from frequency response measurements using rational fraction polynomials. *Proceedings of the 1st IMAC*, 1982.

[14] CG Rodriguez, Eduard Egusquiza, Xavier Escaler, QW Liang, and François Avellan. Experimental investigation of added mass effects on a francis turbine runner in still water. *Journal of Fluids and Structures*, 22(5):699–712, 2006.

[15] C.G. Rodriguez, P. Flores, F.G. Pierart, L.R. Contzen, and E. Egusquiza. Capability of structural acoustical fsi numerical model to predict natural frequencies of submerged structures with nearby rigid surfaces. *Computers & Fluids*, 64:117 – 126, 2012.

[16] Eric J. Ruggiero, Gyuhae Park, and Daniel J. Inman. Multi-input multi-output vibration testing of an inflatable torus. *Mechanical Systems and Signal Processing*, 18(5):1187 – 1201, 2004.

[17] Charles Seeley, Andre Coutu, Christine Monette, Bernd Nennemann, and Hugues Marmont. Characterization of hydrofoil damping due to fluid-structure interaction using piezocomposite actuators. *Smart Materials and Structures*, 21(3):035027, 2012.

[18] H. Tanaka. Vibration behavior and dynamic stress of runners of very high head reversible pump-turbines. In *IAHR Symposion*, Belgrade 1990.

[19] D. L. Thomas. Dynamics of rotationally periodic structures. *International Journal for Numerical Methods in Engineering*, 14(1):81–102, 1979.

[20] Chirag Trivedi. A review on fluid structure interaction in hydraulic turbines: A focus on hydrodynamic damping. *Engineering Failure Analysis*, 77(Supplement C):1 – 22, 2017.

[21] Chirag Trivedi and Michel J. Cervantes. Fluid-structure interactions in francis turbines: A perspective review. *Renewable and Sustainable Energy Reviews*, 68(Part 1):87 – 101, 2017.

[22] David Valentin, David Ramos, Matias Bossio, Alexandre Presas, Eduard Egusquiza, and Carme Valero. Influence of the boundary conditions on the natural frequencies of a francis turbine. *IOP Conference Series: Earth and Environmental Science*, 49(7):072004, 2016.

[23] David Valentín, Alexandre Presas, Eduard Egusquiza, Carme Valero, and Matias Bossio. Dynamic response of the mica runner. experiment and simulation. *Journal of Physics: Conference Series*, 813(1):012036, 2017.

[24] Zhifeng Yao, Fujun Wang, Matthieu Dreyer, and Mohamed Farhat. Effect of trailing edge shape on hydrodynamic damping for a hydrofoil. *Journal of Fluids and Structures*, 51:189 – 198, 2014.

## Appendix

Below are all of the measured frequency response curves provided

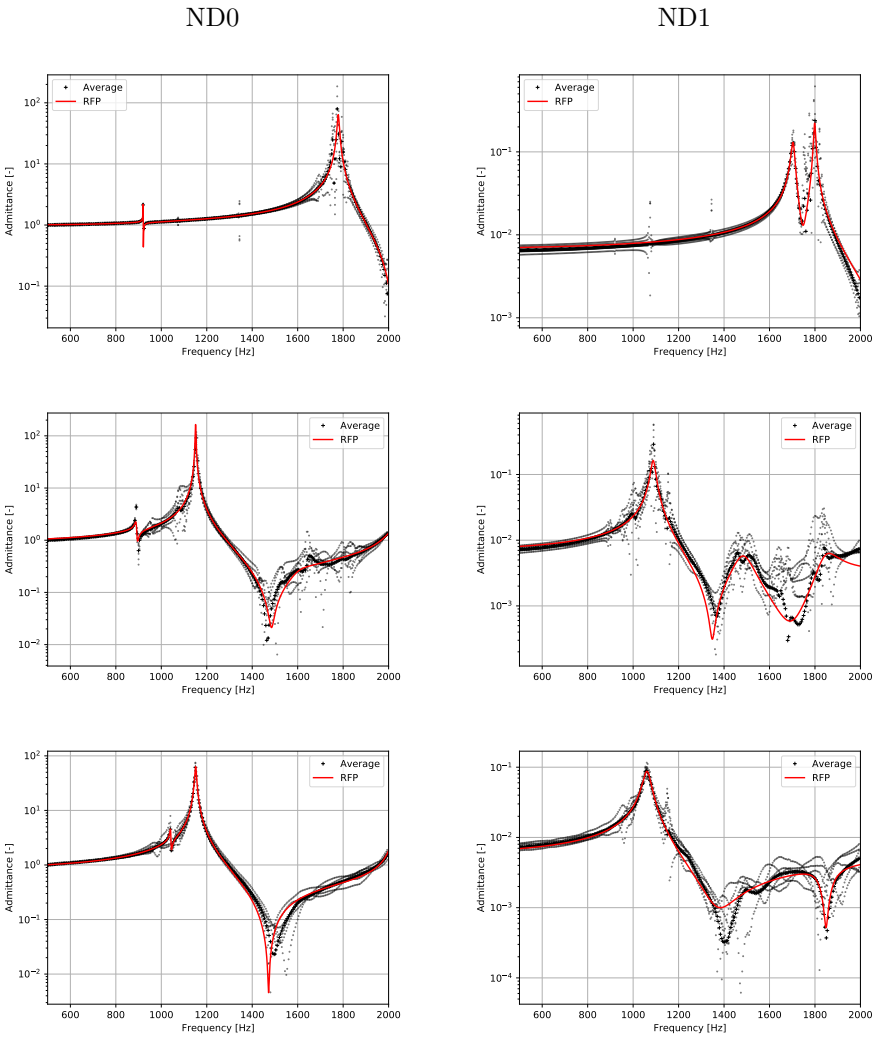


Figure 8: Frequency response of the runner for ND0 amd ND1 for three differet setups: Air - Water - Housing

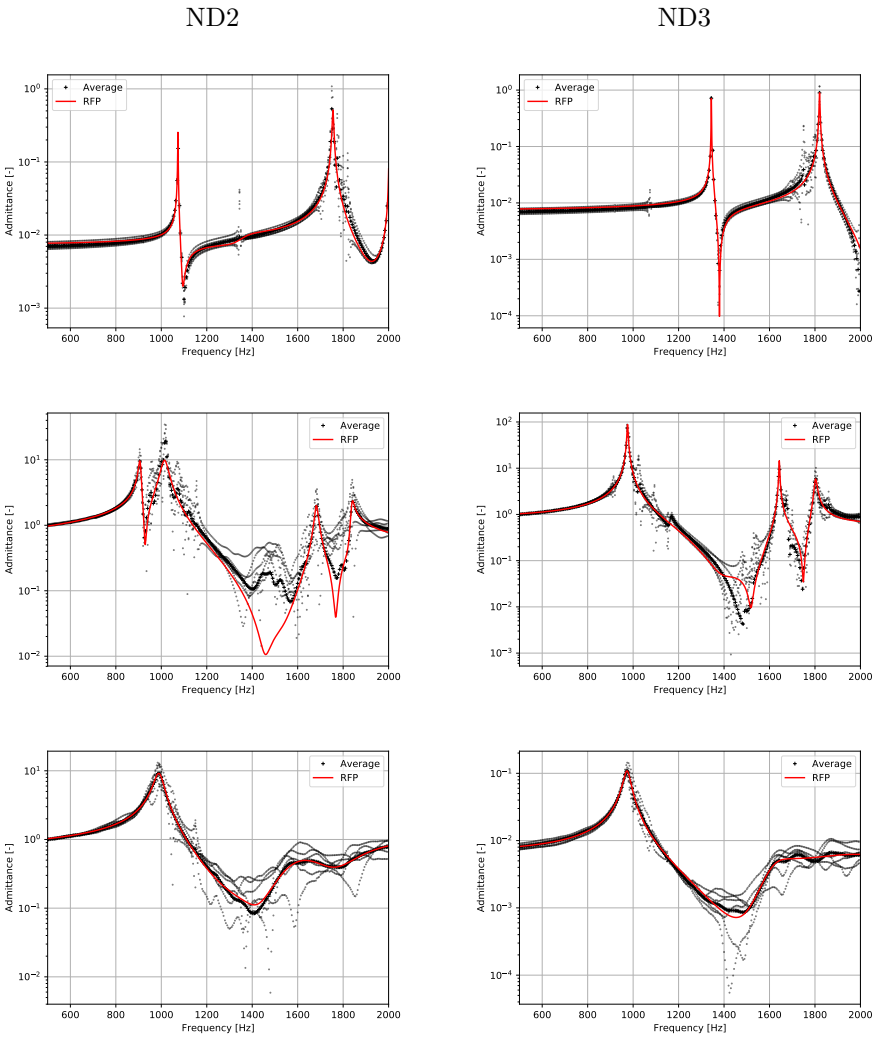


Figure 9: Frequency response of the runner for ND2 amd ND3 for three differet setups: Air - Water - Housing